Viscosity of blood at the microscale infected by *Plasmodium falciparum*

Author: Nil Masó Castro*
Màster en Física dels Sistemes Complexos i Biofísica.
Facultat de Física, Universitat de Barcelona, Martí i Franquès 1, 08028 Barcelona, Spain.†

Advisors: Aurora Hernández Machado[1], Hernando A. del Portillo[2]
[1] *Departament de Física de la Matèria Condensada.*
Universitat de Barcelona, Carrer de Martí i Franquès, 1, 11, 08028, Barcelona, Spain and
[2] *Institut d'Investigació en Ciències de la Salut Germans Trias i Pujol.*
Ctra de Can Ruti, Camí de les Escoles s/n, 08916, Badalona, Spain
(Dated: June 30, 2023)

Abstract: The viscosity of blood infected by malaria is studied using a microfluidic-based rheometer. Malaria is an infectious disease that causes numerous infectious worldwide, being one of the most prevalent diseases. The findings provide insights into the physical properties of the parasite, with potential implications for malaria diagnostics. The microrheometer allows to perform experiments and obtain the viscosity curve as a function of the shear rate using low volumes of blood, contrary to commercial viscosimeters. The viscosity of blood is well characterized using a power-law model, which only needs two parameters to be defined.

Blood samples in culture media (RPMI) and at a physiological temperature were analysed. Moreover, blood samples infected with *Plasmodium falciparum* with different percentage of infected red blood cells were analyzed. Results show a shift towards a Newtonian behaviour as parasitemia increased, losing the characteristic shear-thinning behaviour of blood. This study also examines the influence of mature parasite stages on blood viscosity, revealing their contribution to the observed changes.

These findings have two implications. Firstly, we enhance our understanding of the rheological alterations caused by malaria infection, which can aid in developing improved diagnostic tools based on rheological markers. Secondly, the surprising results obtained contribute to the knowledge about the effects of the parasite as the sample ages at 37°C, which ultimately could aid the development of new malaria treatment techniques.

Keywords: Malaria, Microfluidics, Viscosity, Hemorheology, Diagnostic

I. INTRODUCTION

Infectious diseases are one of the most broad and relevant research fields in medical health. Throughout history, these diseases have caused epidemics and pandemics, and posed significant challenges to public health. Understanding and effectively managing infectious diseases is crucial for safeguarding public health, reducing healthcare costs and ensuring a sustainable future. In the present, research groups from other scientific branches like physics have specialized in understanding the causes and consequences of these diseases from a physical point of view.

In this work, the focus will be on malaria, which is one of the most commonly known infectious diseases in human history. In 2019, there were over 229 million cases of malaria, making it one of the most prevalent parasitic diseases worldwide [1]. It is caused by the *Plasmodium* genus, a group of unicellular eukaryote organisms that parasite a wide range of living beings. These species depend on blood-feeding insects like mosquitoes, that in the course of blood meal they inject these parasites into the human body bloodstream, for instance. The most common mosquito species for malaria transmission is the *Anopheles*, which serves as a host for *Plasmodium falciparum* (*Pf*) and *Plasmodium vivax* (*Pv*) species, both which can cause severe and fatal infections if not treated properly. *Pf* is responsible for more human deaths, whereas *Pv* is more widespread over the world.

In Fig. 1 the different stages of the asexual malaria cycle can be seen, which comes after the pre-erythrocytic human infection (this occurs just after the mosquito bite). In this stage the injected sporozoites travel to the liver in order to invade the hepatocytes (liver cells) and create the parasitophorous vacuole, a process that takes between 10 and 12 days. When the hepatocyte is fully infected it will release up to 40.000 merozoites again into the bloodstream.

Merozoites is the blood-stage parasite that will invade healthy red blood cells (RBCs) and begin the asexual erythrocytic stage shown in Fig. 1. The RBCs will work as a host cell that throughout this asexual stage will increase the number of parasites in the erythrocyte. The invasion is done with receptor and ligand interactions between the parasite and host RBC surface, and some antigens released by the parasite can induce changes in the host cell before the invasion, facilitating the para-

* nmaso14@gmail.com
† master.complex.biophys@ub.edu

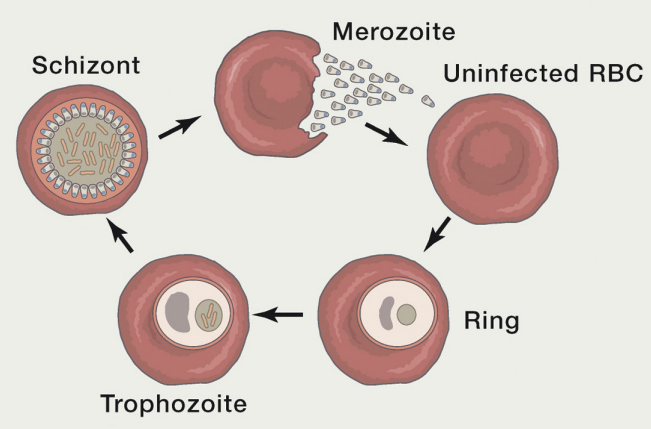

FIG. 1. The asexual erythrocytic stage of malaria, for the *Plasmodium falciparum* and *vivax* species. This stage lasts approximately 48 hours for both species. Image extracted from [2].

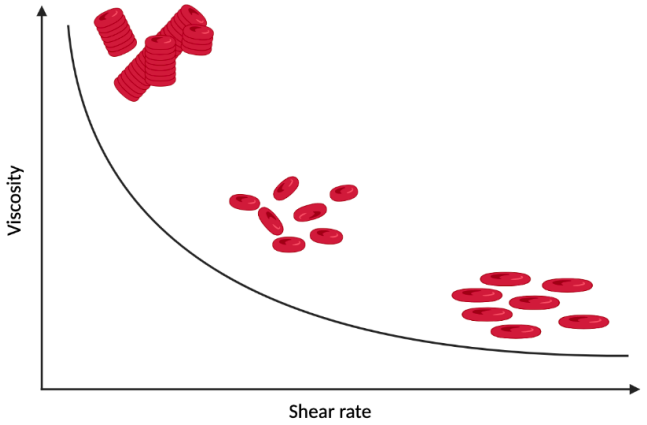

FIG. 2. Qualitative plot of the viscosity of blood as a function of the shear rate applied. The three different shear rate regions are shown with a visual representation of the RBCs arrangements and morphological changes. Image adapted from [8].

sitation of the RBC [3] [4]. After infection, the parasite will start the ring stage and during the subsequent 48 hours it will increase in size to become a trophozoite and finally a schizont. During this development, the parasite consumes the RBC resources in order to induce cell division and create new merozoites. Each schizont stage RBC holds up to 40 merozoites, which will destroy the RBC and cause a rapid release of all merozoites into de bloodstream to invade new RBCs. This process has a low efficiency since not all the released merozoites will infect new RBCs; approximately, each infected red blood cell (iRBC) that undergoes the full asexual cycle, when breaking the membrane (lysis), will infect up to 6 new RBCs.

Aside from the asexual cycle, a proportion of the merozoites will undergo a sexual stage to develop female and male gametocytes. These differentiated RBCs, after maturation inside the bone marrow, will enter peripheral circulation to then be ingested by a mosquito. Finally, after the sporogonic cycle, the created sporozoites will stay in the salivary glands ready to be injected into a new living being [2].

Nowadays, scientists can cultivate the *Pf* parasite *in vitro* and control its stage in the asexual cycle in order to study this organism more deeply.

The consequences and symptoms of malaria depend on the *Plasmodium* species considered. Generally, malaria causes fever, headaches, nauseas and overall fatigue, to name a few. However, it can cause complications like severe anemia (small amount of erythrocytes in the blood), cerebral malaria (infected erythrocytes clog the brain blood vessels), thrombocytopenia (small amount of platelets in the blood), etc. Additionally, this disease can worsen the health condition of pregnant women, since both the mother and the unborn child are more endangered when exposed to this infection.

With the aim of understanding this disease from a physical point of view, hemorheology is introduced, which is the study of blood flow and its viscoelastic properties. For instance, the deformability of RBCs is determined by the intracellular viscosity (hemoglobin inside and structure) and the membrane flexibility, and can be studied using a large variety of methods [5]. However, in this study we focus on the viscosity of this biofluid, which relies on various factors: the hematocrit (the volume percentage of RBCs in the blood), the deformability and elasticity of RBCs and the plasma viscosity [6]. Also, blood viscosity, which increases with higher hematocrit, is considered as an important determinant for oxygen transport and delivery [7].

Additionally, the applied shear rate, representing the rate at which tangential force is exerted, affects the viscoelastic properties of RBCs and their aggregation.

In Fig. 2, the range of viscosity values is related to a different configuration of aggregation and deformability of RBCs. At low deformations, the high viscosity is associated to the aggregation of RBCs in *rouleaux*, which are stacks of RBCs that pile up due to entropic forces and adhesive proteins in the blood [9]. As the shear rate is increased, the rouleaux are less probable to form and hence, the viscosity decreases. For high shear rates, the RBCs struggle to aggregate and due to the large deformation the RBCs tend to deform (elongate), decreasing the viscosity even more. This non-linear behaviour is also known as shear-thinning behaviour, since as you increase the shear rate applied the viscosity decreases.

After the *Plasmodium* parasite invasion, the iRBC undergoes numerous viscoelastic changes, thereby altering the rheological properties of the entire blood. The rigidity and flexibility of the IRBCs are dependent

on the specific species of *Plasmodium* involved. This relationship has been demonstrated in [10], which provides evidence that as the parasite matures, *Pf* infected RBCs (*Pf*-iRBCs) become more rigid, while *Pv*-IRBCs exhibit twice the flexibility. Furthermore, it has been observed that as the *Pv* parasite matures, it tends to enhance the surface area of the reticulocytes, young RBCs representing the host cell for this *Plasmodium* species.

The methods proposed in this work allow us to obtain the viscosity of blood using a microfluidic device. These devices play a crucial role in examining blood viscosity and its alterations at the microscale. They also enable precise and accurate measurements using minimal volumes of blood, which is always beneficial for a possible future application of this technology in hospitals.

Many papers study the deformability of the RBC when infected with malaria by using different techniques [11], nevertheless no experimental studies on the viscosity of blood infected by malaria have been performed at the microscale. By comparing the viscosity values of healthy and *Pf* infected blood, we would be able to diagnose malaria early in the infection, when the patient is still not showing symptoms. Moreover, the effect of temperature in the sample is studied in order to compare the changes in the viscosity.

II. MATHEMATICAL MODEL

In order to compute the viscosity of blood from the data obtained of pressures and velocities, a mathematical model is needed, considering the geometry and the conditions of the microfluidic system shown in Fig. 3A. This is mathematical derivation partly based on [12].

The shear rate is the gradient of velocities of the fluid when applying a certain stress, and it is defined as:

$$\dot{\gamma}(z) = \frac{\partial v_x}{\partial z} \,, \tag{1}$$

considering the spatial coordinates in Fig. 3A. At different heights of the fluid front the velocity of each layer is different due to the friction between the layers (the viscosity).

To describe the fluid behaviour inside the microchannel a full derivation of the momentum equations is needed. Starting with the Cauchy momentum equation for incompressible fluids:

$$\rho \frac{D\vec{v}}{Dt} = -\vec{\nabla} P + \vec{\nabla} \cdot \vec{\tau} \,, \tag{2}$$

where ρ is the density of the fluid, $\vec{\nabla} P$ is the gradient of pressure and $\vec{\nabla} \cdot \vec{\tau}$ is the divergence of the shear stress tensor. The left side of Eq. (2) is a material derivative, containing a variation of the velocity field along time and a convective term. Given the geometry of the system and the magnitude of the variables, we can consider stationary conditions and small Reynolds number ($\approx 10^{-3}$), so both terms in the material derivative can be neglected. This is called the Stokes regime, where inertia is not considered. Therefore, Eq. (2) is simplified to:

$$\vec{\nabla} P = \vec{\nabla} \cdot \vec{\tau} \tag{3}$$

The shear stress τ is a symmetrical tensor that when describing incompressible fluids can be expressed as $\tau_{ij} = \eta \left(\partial_{x_j} v_i + \partial_{x_i} v_j \right)$. Considering that the fluid only flows along the x direction $\vec{v} = v_x(z)\hat{x}$, one can derive the x component of τ, and since the only non-zero term is $\partial_z v_x$, the x component of Eq. (3) becomes the following equation for this geometry:

$$\frac{\partial}{\partial z} \left[\eta \, \dot{\gamma}(z) \right] = \frac{\partial P}{\partial x} \tag{4}$$

The gradient of pressure along the x axis can be approximated as a drop in pressure ΔP and the position of the mean fluid front h(t). This fluid front is defined as the mean of all the infinitesimal layers of fluid along the z axis:

$$h(t) = \frac{1}{N} \sum_{n=1}^{N} h_n(t) \tag{5}$$

With Eq. (5), we are treating the fluid-air interference as a fluid front where every point of fluid is advancing at the same speed.

This allows to simplify the derivation of the mathematical expressions, and integrating Eq. (4) we obtain:

$$\eta \, \dot{\gamma}(z) = \frac{\Delta P}{h(t)} z \tag{6}$$

The pressure drop ΔP has three main contributions:

$$\Delta P = P_{pump} - \Delta P_t - \Delta P_c \,, \tag{7}$$

where P_{pump} is the pressure at which the suction pump is sucking out the fluid, ΔP_t is the pressure drop along the microtube and ΔP_c is the capillary pressure. The main contribution to making the fluid to flow is the pressure exerted by the pump. The capillary pressure, which depends on the sample and it is related to the curvature of the fluid front, has a magnitude of only 10^2 of Pa; however, this has to be considered in order to obtain the best possible parameters n and m. Is worth mentioning that the fluid level and the microchannel have an small height difference between them, but it is not considered in these equations since later it will be added as a constant. This is explained in the Methods section.

In order to solve Eq. (6) the viscosity has to be defined. The viscosity of a fluid is the resistance of the material to deformation when applying a shear strain. It is also understood as a transfer of momentum or the friction between infinitesimal layers of fluid. For Newtonian fluids, the response of the fluid or shear stress τ to a certain shear strain rate $\dot{\gamma}$ is described with a linear relation:

$$\tau = \eta\dot{\gamma} \tag{8}$$

Water and blood plasma follow this constitutive equation, where the slope of the straight line is the viscosity. By calculating the slope in each point you obtain the viscosity of the fluid.

However, for non-Newtonian fluids the shear stress is changes when applying a different shear strain rate, so the viscosity is not constant. For these complex fluids we need to define an apparent viscosity, since the relation in Eq. (8) do not hold. This apparent viscosity η_{app}, which will be rewritten as η, is defined as the ratio between the shear stress τ and the shear strain rate $\dot{\gamma}$:

$$\eta_{app} = \frac{\tau}{\dot{\gamma}} \tag{9}$$

The behaviour of Non-Newtonian fluids can be described with a power-law model, which states that the relationship between the shear stress of the fluid when applying a certain shear strain rate is non-linear:

$$\tau = m\dot{\gamma}^n \tag{10}$$

Where the non-linearity comes from the exponent n. Eq. (10) is also known as the Ostwald-de Waele relationship [13], and it is well known empirical approximation to describe the non-linear behaviour of non-Newtonian fluids within a shear rate range.

Now, an equation for the shear rate is obtained by substituting Eq. (9) into Eq. (6), and afterwards substituting the shear stress τ by Eq. (10):

$$\dot{\gamma}(z) = \frac{\partial v_x}{\partial z} = \left(\frac{z}{m}\frac{\Delta P}{h(t)}\right)^{\frac{1}{n}} , \tag{11}$$

where the plane $z = 0$ is perpendicular x (velocity field direction) and is aligned to the middle of the fluid front, so the z coordinate goes from $z = -b/2$ to $z = b/2$, where b is the height of the microchannel. Then Eq. (11) can be integrated with respect to the z coordinate to obtain the velocity profile:

$$v(z) = \frac{n}{1+n}\left(\frac{1}{m}\frac{\Delta P}{h(t)}\right)^{\frac{1}{n}}\left[z^{1+\frac{1}{n}} - \left(\frac{b}{2}\right)^{1+\frac{1}{n}}\right] , \tag{12}$$

where $v_x \equiv v$. For the integration constant in Eq. (12) non-slip boundary conditions have been considered in the top and bottom layers of the microchannel, mathematically written as $v(z = \pm b/2) = 0$.

Although the velocity profile is necessary, the total flow (the volume of fluid flowing for unit of time) has to be defined in order to get rid of any dependences with the z coordinate. The total flow along the microchannel Q_m is:

$$Q_m = \frac{2wn}{1+2n}\left(\frac{b}{2}\right)^{2+\frac{1}{n}}\left(\frac{\Delta P}{mh(t)}\right)^{\frac{1}{n}} , \tag{13}$$

where w is the width of the microchannel.

From the fluid front position $h(t)$ the mean front velocity is defined as $\dot{h}(t)$. Thus, the total flow in the microchannel can be written as $Q_m = bw\dot{h}$.

Considering now Eq. (13), an expression of the total pressure drop is obtained:

$$\Delta P = \left(\frac{2}{b}\right)^{1+n}\left(\frac{1+2n}{n}\right)^{n} mh(t)\dot{h}^n \tag{14}$$

Since we defined a mean front velocity $\dot{h}$, a shear rate related to the mean velocity has to be defined:

$$\dot{\gamma} = \frac{\dot{h}}{b} \tag{15}$$

On the other hand, a similar mathematical approach can be done to compute the velocity profile in the microtube and subsequently obtain the pressure drop ΔP_t when the fluid flows along the microtube. For this geometry, cylindrical coordinates have been considered with the velocity vector going on the z direction (direction along the microtube) and only depending on the radial coordinate r: $\vec{v} = v_z(r)\hat{z}$. Starting from the shear stress tensor τ, now by deriving the z component and considering Eq. (3), an equation for the microtube is obtained:

$$\frac{1}{r}\frac{\partial}{\partial r}\left[r\frac{\partial v_z}{\partial r}\eta\right] = \frac{\partial P_t}{\partial z} \tag{16}$$

In a similar way, one can approximate the gradient of pressure along the microtube as $\partial_z P_t = \frac{\Delta P_t}{l_t}$, where l_t is the length of the microtube. Here, the position of the fluid front has no meaning since the experimental measurements are performed after the microtube is completely filled.

Following a similar mathematical procedure than when deriving the equations for the microchannel, the total flow in the microtube Q_t is obtained:

$$Q_t = \pi r_t^{3+\frac{1}{n}}\left(\frac{n}{1+3n}\right)\left(\frac{\Delta P_t}{2ml_t}\right)^{\frac{1}{n}} \tag{17}$$

In Eq. (17), r_t is the radius of the microtube. The total flow in the microtube can be also written as $Q_t = \pi r_t^2 v_t$, where v_t is the mean velocity along the microtube. By equalizing the two equations for Q_t an expression for the pressure drop along the microchannel is obtained:

$$\Delta P_t = \left(\frac{1}{r_t}\right)^{1+n}\left(\frac{1+3n}{n}\right)^{n} 2ml_t v_t^n \tag{18}$$

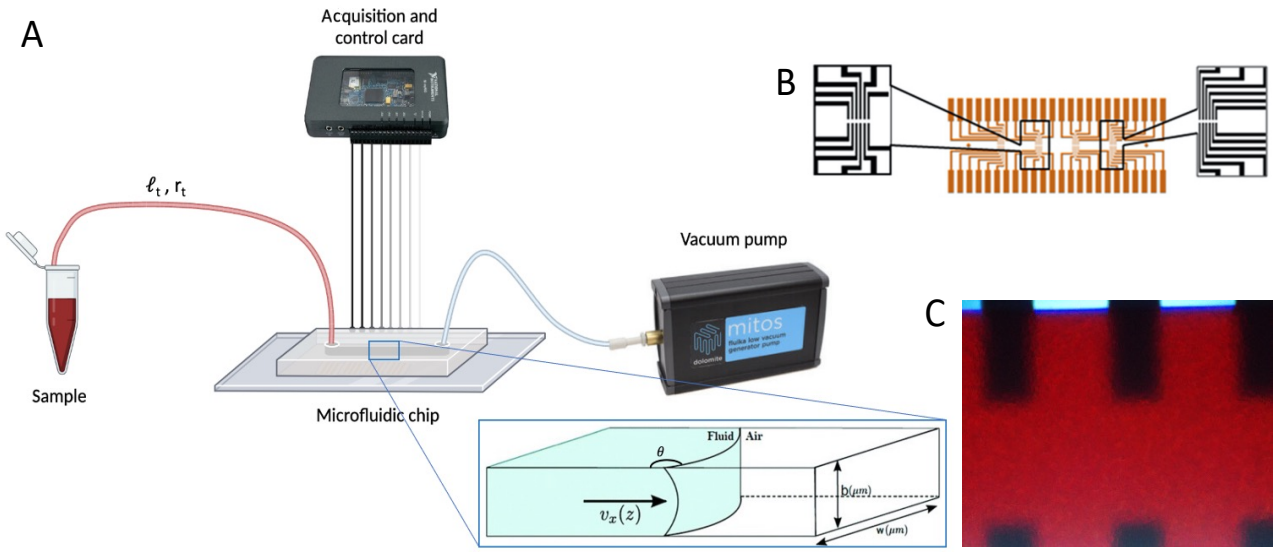

FIG. 3. **A:** Schematic representation of the experimental set-up. The vacuum pump suctions the liquid from the sample reservoir and flows the liquid through the microtube (r_t, l_t) and the microchannel (b, w). The data is obtained with an acquisition card that also controls the set-up. A representative zoom (extracted from [6]) shows the liquid-air interface in more detail. **B:** Top view of the microfluidic chip, with the arrangement of electrodes. Image extracted from [14]. **C:** Image of the microfluidic chip filled with blood, which looks like a gel material. Image taken with a Nikon DS-Fi2 camera mounted on a Nikon ECLIPSE Ci microscope.

Since the fluid that goes through the microtube goes directly to the microchannel without any liquid leakage, a mass conservation law can be defined using the total flow in each of these regions: $Q_m = Q_t$, where

$$bw\dot{h} = \pi r_t^2 v_t \tag{19}$$

Eq. (14) and Eq. (18) can be substituted into Eq. (7), and considering Eq. (19) one obtains:

$$\dot{h}^n = \frac{P_{pump} - \Delta P_c}{\left[\left(\frac{wb}{\pi r_t^2}\left(\frac{1+3n}{n}\right)\right)^n \frac{2ml_t}{r_t^{1+n}} + \left(\frac{2}{b}\right)^{1+n}\left(\frac{1+2n}{n}\right)^n mh(t)\right]} \tag{20}$$

The complexity of Eq. (20) can be reduced by considering the height of the microchannel. Within the denominator, we find two terms: the first term scales with b raised to the power of n ($\propto b^n$), while the second term scales with the inverse of b raised to the power of $n+1$ ($\propto b^{-(n+1)}$). To eliminate the dependence on $h(t)$, a large value of b is required. When the height of the microchannel is sufficiently large, the first term in the denominator becomes significantly smaller compared to the second term, allowing it to be disregarded. This phenomenon occurs because the resistance within the micro-tube is greater than that within the microchannel.

By rearranging the terms in Eq. (20), the relationship between the pressure and the fluid front velocity is obtained:

$$P_{eff} = \frac{2l_t}{r_t^{1+n}}\left[\left(\frac{1+3n}{n}\right)\frac{wb}{\pi r_t^2}\right]^n m\dot{h}^n\,, \tag{21}$$

where the effective pressure P_{eff} has been defined as $P_{pump} - \Delta P_c$. From Eq. (21), the desired parameters n and m can be obtained with a proper fit of the experimental data.

One could argue that the velocity of the mean fluid front could change as the microchannel is being filled, but researchers using a similar set-up found out that this velocity is constant in a certain regime [15]. Outside the so-called Washburn regime, the relationship between the position of the fluid front along time is linear, meaning that the velocity of advancement is constant. By increasing the height of the microchannel and having an small enough radius of the microtube, this linear regime stays for longer, avoiding any issues when using the mathematical equations obtained.

Finally, by substituting Eq. (10) into Eq. (9), the equation for the viscosity of a non-Newtonian fluid is obtained:

$$\eta = m\,\dot{\gamma}^{n-1} \tag{22}$$

Eq. (22) allows us to describe the viscosity of blood with this very simple model, which is widely used in rheology, as it provides a very good approximation of the

viscosity using only 2 parameters. These 2 parameters have different contributions to the viscosity of the fluid:

- Flow behaviour index n: dimensionless number that describes the change of viscosity when varying the shear rate applied.
- Flow consistency coefficient m: its dimensions depend on n, $[m] = Pa \cdot s^n$. Describes the change of viscosity due to the colloidal content in the sample.

Depending on the value of the flow behaviour index, the fluid can have 3 different types of behaviour. If $n = 1$ the fluid is Newtonian, since the viscosity is directly m and does not depend on the shear rate, it is constant. If $n > 1$ the fluid is shear thickening, as the viscosity increases as we increase the shear rate. Finally, if $0 < n < 1$ the fluid is shear thinning, since the viscosity decreases with increasing shear rate applied. The determination of these exponents will allow us to obtain the viscosity of any fluid when applying a certain shear rate. Blood, as mentioned before, is a shear thinning fluid so the results should show a flow behaviour index lower than 1. In the case of blood plasma, a $n = 1$ result is expected.

Other models like the Carreau-Yasuda model have been considered, but discarded due to the higher number of constants that have to be obtained. The power-law model only has 2 constants that can be easily obtained with the proper curve fitting algorithm.

III. METHODS

A. Sample preparation

All the experiments in this study were performed at the Plasmodium vivax and Exosomes group (PVREX) within the Germans Trias i Pujol Research Institute (IGTP). This research group is specialized in studying the *Plasmodium* parasite, and their facilities are equipped with the necessary instruments to conserve and incubate the parasite under optimal conditions. Moreover, their laboratory technicians have years of experience in handling parasite cultures and sample preparation.

The samples analysed in this study came from an specific *Pf* strain called 3D7. The parasite cultures were inside an incubation chamber, sitting in culture flasks with healthy RBCs at 37°C. This condition is ideal since the parasite will easily invade RBCs at human temperature, which is their optimal environment. It is worth mentioning that the blood used in the laboratory is reestablished approximately every three weeks, so the effect of blood ageing when conserving the blood could alter the results obtained. The analysed samples consisted on Eppendorf tubes containing a blood volume between 400 and 600 μl.

In order to study the malaria parasite in different stages of the disease, they cultivate the iRBCs with a cell culture medium called RPMI, which contains amino acids, vitamins and phosphate molecules. These components allow the proper growth of blood cells *in vitro*. However, this medium could also alter the viscoelastic properties of the RBCs and consequently change the viscosity of blood. For a more realistic situation, the iRBCs of some samples have been resuspended in blood plasma in order to study the effect of RPMI on viscosity.

The hematocrit for human blood ranges from 36% to 50%, depending on the subject and the gender. For the analysed samples, the hematocrit was settled to 40%, which is resemblant to the RBCs volume in endemic regions like Africa. Nevertheless, the parasite cultures are at *circa* 3% of hematocrit, thus healthy RBCs are added to the sample in order to reach an hematocrit of 40%. At this hematocrit, the non-linear behaviour of blood viscosity should be noticeable, given that at low hematocrits it exhibits a Newtonian behaviour [12].

With the view of studying the viscosity of blood when infected by the different stages of the asexual cycle of *Pf*, the parasite needs to be synchronized. This is done using sorbitol, a sugar alcohol that when added to a blood sample will induce erythrocyte lysis only on the trophozoites and schizonts (mature stages). This differentiation is caused by the increased osmotic fragility of the mature stages, causing an influx of liquid that leads to the membrane breakage [16]. Thus, by adding sorbitol to an unsynchronized culture, only the iRBCs in the ring stage will persevere. The whole asexual cycle lasts 48 hours, so measurements of the same parasite stage were done every 2 days, seeing that a synchronized culture in ring stage would be in mature stages in approximately 24 hours.

Another important variable for this study is the parasitemia, which is the percentage of RBCs that are parasitized. This gives us an idea of how much parasite there is in the sample. The parasitemia estimation is obtained with the counting of iRBCs in staining blood smears. A little drop of the sample is deposited on a glass plate; then, by staining the sample with Giemsa (a series of tints) and applying a shear force to allow drying, the nucleus of the parasite can be seen using a microscope. The parasite staining is caused by the colouring of the hemozoin crystal, an iron subproduct produced by the *Pf* when metabolizing the RBC hemoglobin. In Fig. 4C, the small hemozoin crystals of two ring stage iRBCs can be seen. As the parasite matures, the hemozoin crystal is more noticeable since its size increases; also, the RBC membrane faints due to the lack of hemoglobin. So the parasitemia percentage is obtained by counting the infected and healthy RBCs within a view field and then

computing the ration between the number of iRBCs and the total RBCs, and multiplying by 100.

Is worth mentioning that every 1 or 2 days, the culture medium had to be changed in order to avoid self-destruction of the parasite. The removal of debris and the remnants of RBC membranes that lysed is necessary in order to have an optimal development of the parasite in the culture. However, this change of medium could alter the viscosity of the final sample.

B. Experimental set-up

An image of the experimental set-up is shown in Fig. 4A, which is schematically presented in Fig. 3A. The microrheometer consists of several parts that will allow us to obtain mean front velocity values for different pressures applied.

The microfluidic chip is made of polydimethylsiloxane (PDMS) attached to a glass substrate, creating a microchannel where the fluid front will flow. This attachment was made using plasma bonding between the two materials. But before the bonding, 24 pairs of gold electrodes were imprinted on the glass substrate, with the pattern shown in Fig. 3B. The electrodes are organized in 4 groups of 6 electrodes each, and the electrodes from the same group are spaced a distance d_{elec} (Table I). These pairs of electrodes will detect the fluid front advancement by connection between every pair. When the fluid is in contact with the two electrodes of a pair, an electrical signal will be detected and the fluid front position will be known. By measuring the time between pairs of electrodes, the velocity can be easily obtained.

The orange device shown in Fig. 4A holds the microfluidic chip in place during each measurement. It contains an array of 48 electrical pins that will make contact with the chip when the experimental set-up is ready to measure. These pins are connected to a National Instruments myRIO card (NI), which is a portable device that allow us to obtain the electrical signals detected, but also to control the different parts in the set-up.

The suction of the blood inside the Eppendorf is performed by a Mitos Fluika low pressure vacuum pump, that can apply pressures ranging from 500 Pa to 9000 Pa. The suction pump and the NI are both connected to a laptop The initiation of each measurement is controlled using a user interface, a computer program made with LabView that allows the user to determine the desired suction pressure and to see an schematic representation of the fluid front advancement. Thanks to the NI, after each measurement the program gives the possibility to save the data into a TXT file, which contains the pressure in each step of time and the time that the fluid front needs to reach every pair of electrodes.

TABLE I. Values of the geometrical parameters in the experimental set-up.

Microchannel height, b	325 μm
Microchannel width, w	850 μm
Distance between electrodes, d_{elec}	350 μm
Microtube length, l_t	20 cm
Microtube radius, r_t	127 μm

After each measurement for a determined pressure, the blood inside the microtube and the microchannel was removed using syringes. First, a syringe with MiliQ (highly deionized water) was applied to both parts, to remove as much blood as possible. Then, oxygenated water (H_2O_2) was applied using another syringe, causing lysis to the erythrocytes so the remaining RBCs are removed. In order to avoid lysis in the next measurement, MiliQ is again pumped to remove all the oxygenated water inside these geometries. Finally, all the liquid is removed by using a dry syringe. To ensure that the microchannel is fully dry, the microfluidic chip is deposited over a Thermo Scientific Cimarec$^+$ Hot Plate at 45°C. Afterwards, some time was needed for the decrease of temperature of the chip, so it reaches room temperature.

In each measurement, the blood volume consumed is approximately 20 μl (considering that the microchannel is filled up to 4 cm in length). Since for every sample a set of 7 or 8 different pressures were needed, the total amount of blood in each sample is estimated in 180 μl. The value is overestimated because sometimes the measurement was erroneous. This is was probably caused by the aggregation of RBCs due to sedimentation. The RBCs are very heavy compared to the plasma and other components in the blood, so the erythrocyte sedimentation rate (ESR) is very high creating blood clots in the bottom of the Eppendorf. To remove these aggregations, the samples were on a rotating shaker between measurements, which constantly homogenizes the blood sample.

In addition, when analysing samples at 37°C, the temperature was preserved using a LabNet Dry Bath incubator, which can hold the Eppendorf at the desired temperature. Because of this, these measurements done at a certain temperature were not in constant rotation, but were properly agitated before each measurement to avoid accumulation of RBCs.

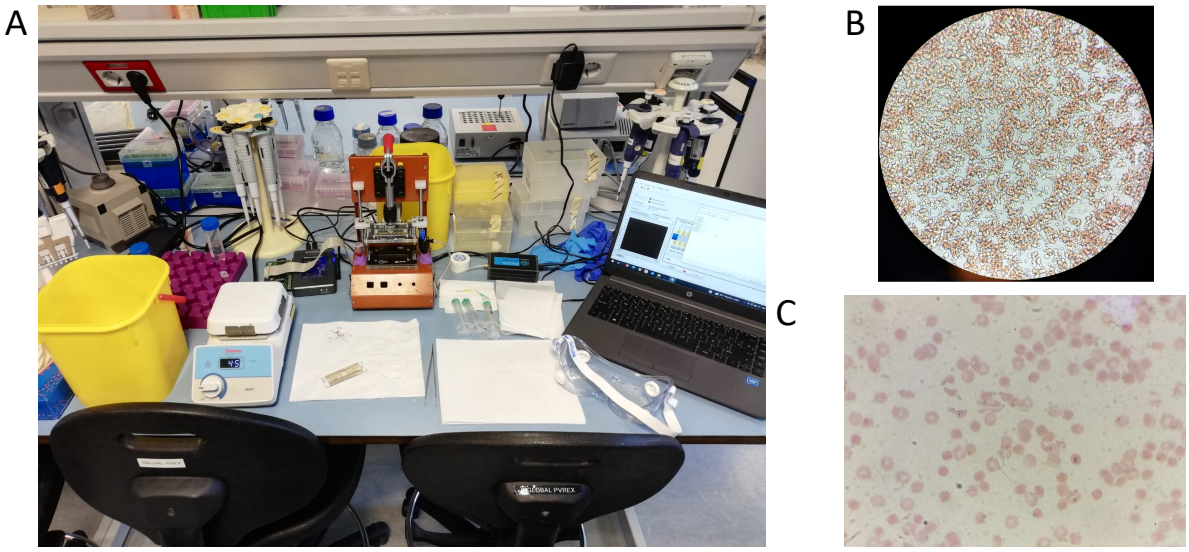

FIG. 4. **A:** Image of the experimental set-up, corresponding to the schematic representation in Fig. (3)A. **B:** Image of an extended drop of blood, where aggregation is seen. Additionally, stacks of RBCs (*rouleaux*) can be seen. Image obtained using a Nikon ECLIPSE Ci microscope. **C:** Image of an smeared glass plate, containing infected and healthy RBCs. Two ring stage iRBCs can be seen thanks to the Giemsa tint, that stains the RBC membrane and the parasite. Image taken with a Nikon DS-Fi2 camera mounted on a Nikon ECLIPSE Ci microscope.

C. Data processing

The creation of a Python code was essential to process all the data automatically. This code allows the user to obtain the desired plots by specifying the directory route where the TXT files are located. The output plots are the effective pressure P_{eff} versus the mean front velocity $\dot{h}$ and the viscosity η versus the shear rate $\dot{\gamma}$. With these plot, a full rheological characterization of the blood is obtained. This script was created with the Spyder environment, and it uses the following modules and libraries: NumPy, SciPy, Pandas, Matplotlib and Os.

With the TXT files obtained from the microrheometer, the mean front velocity is computed as:

$$\dot{h} = \frac{d_{elec}}{\Delta t} \,, \tag{23}$$

where d_{elec} is the distance between the electrodes in each group of six electrodes, and Δt is the time difference between two consecutive electrodes in the same group. The value of d_{elec} is known (shown in Table I), but Δt is computed from the time measurements stored in the TXTs. By averaging over all the velocity values in the 4 groups of 6 electrodes, a mean front velocity is obtained. The error in $\dot{h}$ is obtained through propagation of errors of the standard deviation of the Δt.

To compute the pressure of the pump, a mean of all the pressure values is done, and its error is obtained by calculating the standard deviation. This mean pressure is denoted as P_{pump}, from which the effective pressure P_{eff} will later be obtained.

The experimental values of Δt and P_{pump} were improved by removing the possible outliers using the interquartile range (IQR) method. The IQR is the difference between the third quartile (Q3) and the first quartile (Q1) of the input data, and using this range a maximum $(Q3 + IQR)$ and minimum $(Q1 - IQR)$ bounds can be defined. Thus, this method consists in removing the data values that are outside of the range defined by these bounds, highly improving the mean and standard deviation.

All the results and codes created during this study were uploaded to a private GitHub repository to improve organization and to have an online backup.

D. Curve fitting and computation of viscosity

From the experimental data obtained, the desired n and m parameters can be obtained with an appropriate power-law curve fit.

The data points of mean pressure of the pump P_{pump} and mean front velocity $\dot{h}$ are plotted with a view to fit the data to Eq. (21). Since $P_{eff} = P_{pump} - \Delta P_c$, Eq. (21) can be rewritten as:

$$P_{pump} = K\dot{h}^n + C \tag{24}$$

where K has been defined as:

$$K = \frac{2l_t}{r_t^{1+n}} \left[\left(\frac{1+3n}{n} \right) \frac{wb}{\pi r_t^2} \right]^n m \tag{25}$$

The C term in Eq. (24) accounts not only for the capillary pressure, but also for any extra pressure variations like the hydrostatic pressure caused by a height difference between the microchannel and the liquid level in the Eppendorf.

The needed parameters K, n and C are obtained by employing the Optimize and ODR packages, coming from the SciPy library. Both packages are widely used in the scientific community due to their easy usage and very accurate results, hence they were implemented in the Python code. Moreover, both methods give an error associated to each estimated parameter.

SciPy Optimize uses a non-linear least squares method to fit the function of interest to the data provided. Inherently, it minimizes the deviations from the fit only in the response variable, that in this case is the pump pressure P_{pump}. By defining a initial values of the parameters, the functions in the package perform many iterations trying to obtain the parameters that minimize the vertical distance between the experimental data and the fit. Nevertheless, to obtain better parameters, a method that also considers the horizontal distance between the points and the fit is desirable. Also this package does not consider an error in the x-axis, so we are also losing information about the error in the mean front velocity $\dot{h}$.

The ODR package is more accurate in this case, since it performs an orthogonal distance regression (ODR), a fitting method developed by P. Boggs and J. E. Rogers [17]. This method consists in minimizing the sum of the squares of the orthogonal distance between the experimental data and the fit, so it also considers the horizontal distance. The parameters obtained are very precise because these estimators maximizes the likelihood function, while minimizing the sum of the squares. Furthermore, the ODR package allows us to input the errors in the dependent and independent variables (velocity and pressure, respectively) to improve the parameters obtained.

Following the estimation of K, n and C, the C parameter is subtracted from P_{pump} to obtain the effective pressure P_{eff}. Thereupon, another fit is performed to obtain new K and n parameters. This data is fitted to the following power-law:

$$P_{eff} = K\dot{h}^n \tag{26}$$

The expression in Eq. (26) will fit the experimental data more accurately, but their values will not be as different as from the previously obtained parameters.

From the values of K and n, the m coefficient is obtained by dividing K by the whole prefactor preceding m in Eq. (25). Besides the parameters, the shear rate is calculated using Eq. (15).

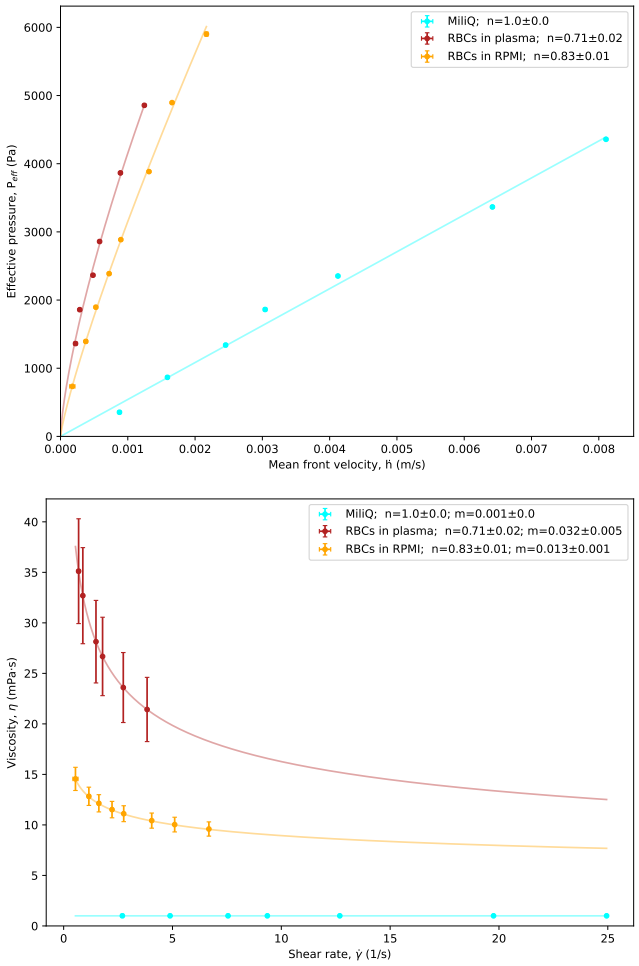

FIG. 5. Plots of the samples analysed to study the effect of RPMI on blood viscosity. The obtained n and m parameters are shown in the legend, along alongside their error. **Top:** Effective pressure P_{eff} as a function of the mean front velocity $\dot{h}$. **Bottom:** Viscosity η as a function of the shear rate $\dot{\gamma}$.

Finally, Eq. (22) is applied to obtain the viscosity for different values of the shear rate $\dot{\gamma}$, using the obtained n and m parameters. The error in the viscosity is obtained from the propagation of errors in the shear rate and in the estimation of n and m.

IV. RESULTS AND DISCUSSION

A. The effects of the culture medium

The viscosity of MiliQ and RBCs in plasma and in the RPMI medium can be seen in the bottom plot of Fig. 5. The viscosity of MiliQ is approximately 1 mPa·s, a value much lower than the viscosities obtained for the blood samples. As expected, water is a Newtonian fluid, so the

top plot of Fig. 5 shows a linear relationship between the pressure (the stress) and the velocity (the strain). This result is shown to see the difference in viscosity between the blood and a simple fluid like water, and affirm that the components of blood (specially RBCs) hugely contribute to the rheological properties of this biofluid.

The non-linear behaviour is clearly seen in the blood samples of Fig. 5. The viscosity values of RBCs in plasma are a bit higher than in other studies, but the n exponent is very similar. However, when changing the plasma for the RPMI medium, the viscosity decreases to half. This medium is widely used in health research groups, which focus on other aspects of their biological samples. Nevertheless, as seen in this section, the contribution of this medium to the rheological properties of blood is massive and when performing a rheological experiment has to be considered.

For both samples, more points for higher shear rates are needed in order to better characterize the viscosity and not only rely on the curve extrapolation using Eq. (22).

From now on, the RBCs in the cultures were removed from the RPMI solution and resuspended in plasma. This was done to avoid the effects of the medium and having a sample that is more resemblant to real blood.

B. The effects of temperature

The effects of temperature on the viscosity of blood have been studied. The human body maintains its temperature around the 37°C, so by measuring the viscosity at this temperature would give us a physiological value of viscosity. It is well known that temperature changes the viscosity of blood. A higher temperature is associated to the cells consuming more energy and supplies to survive. Within these supplies oxygen is very relevant, so a higher amount of oxygen is necessary to keep the cells alive. Therefore at higher temperatures the hemoglobin becomes less likely to bind to oxygen, and consequently, when considering the human microvascular system, these oxygen molecules cannot be properly unloaded into the cells of any tissue [18].

In the top plot of Fig. 6, a decrease in the slope can be seen, so there will be a difference in viscosity between the two samples. This is shown in the bottom plot, which show that the viscosity decreases as you increase the temperature of the sample.

C. Early diagnostic of malaria infection

In this section we wanted to study if a diagnostic of *Plasmodium falciparum* parasitation in ring stages at low parasitemias in early stages of infection was possible. If any difference in viscosity is shown between ring stages at

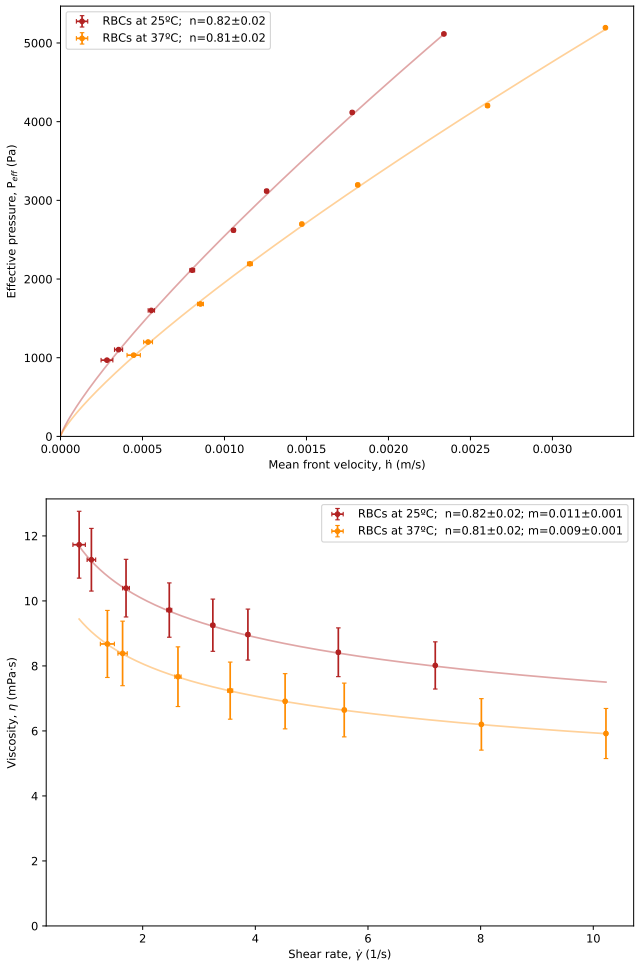

FIG. 6. Plots of the samples measured at 25°C and 37°C. The obtained n and m parameters are shown in the legend, alongside their error. **Top:** Effective pressure P_{eff} as a function of the mean front velocity $\dot{h}$. **Bottom:** Viscosity η as a function of the shear rate $\dot{\gamma}$.

low parasitemias and healthy blood, an early diagnostic of the infection could be possible. This could be done by comparing the viscosity curves of non-infected and infected blood, emphasising the difference in the value of the n exponent and the position of the whole curve in the y-axis.

To ensure that the parasites were at rings stage, the measurements were taken every 2 days since the parasite goes through its whole asexual cycle every 48 hours. Two similar experiments with same parasitemias were performed in order to compare the results.

In the bottom plot of Fig. 7 we can see how the viscosity decreases as the parasitemia increases, as the amount of rings in the sample increase. Moreover, the value of n approaches a Newtonian behaviour of liquid, where the pressure and the velocity have a linear relationship. This is an interesting and surprising result, since, from the literature, we know that *Pf* parasite tend to increase the

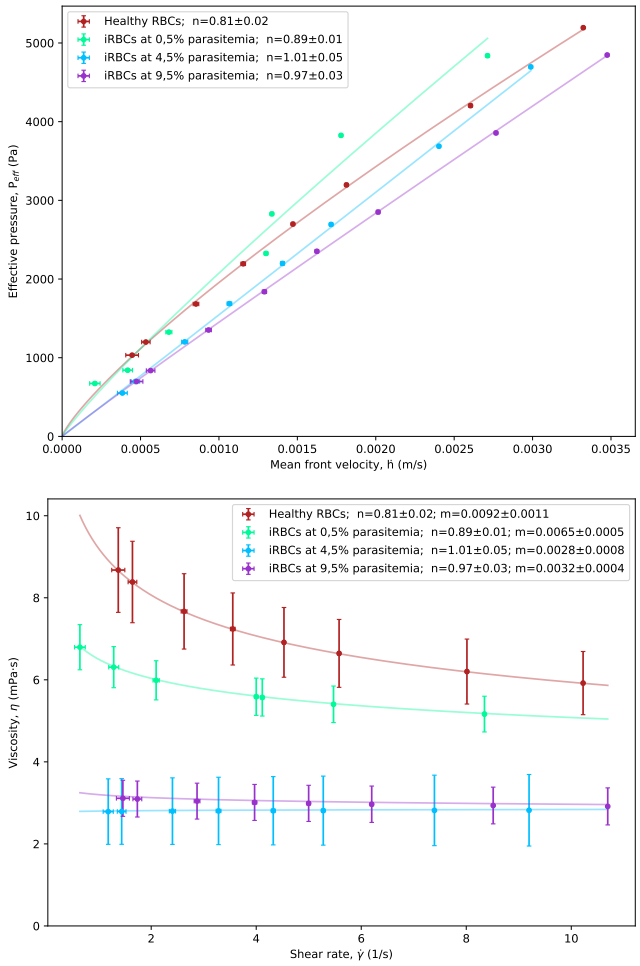

FIG. 7. Plots of the first experiment performed when studying the effect of the ring stage RBCs in the viscosity. The obtained n and m parameters are shown in the legend, alongside their error. **Top:** Effective pressure P_{eff} as a function of the mean front velocity $\dot{h}$. **Bottom:** Viscosity η as a function of the shear rate $\dot{\gamma}$.

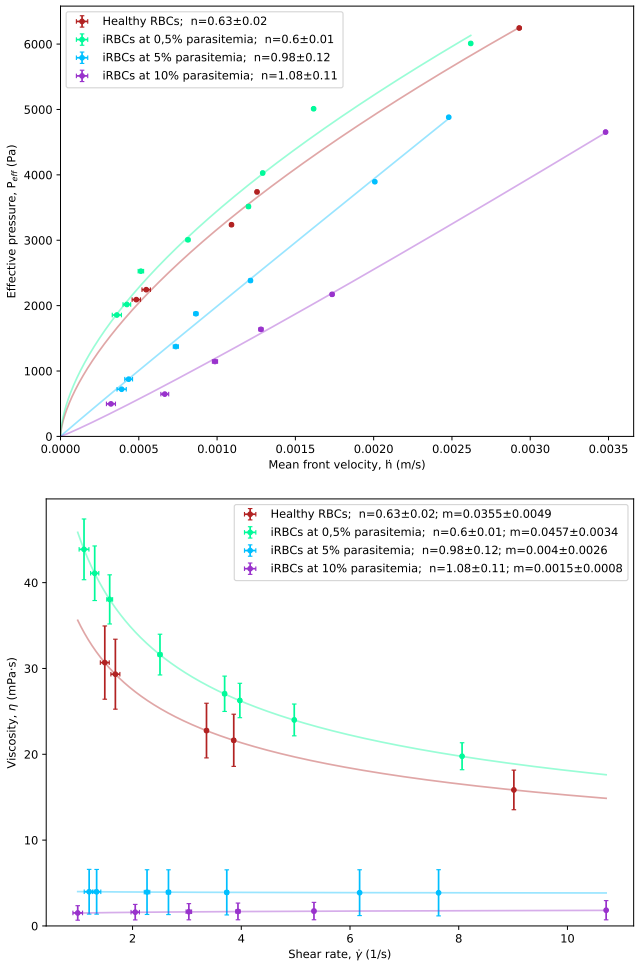

FIG. 8. Plots of the second experiment performed when studying the effect of the ring stage RBCs in the viscosity. The obtained n and m parameters are shown in the legend, alongside their error. **Top:** Effective pressure P_{eff} as a function of the mean front velocity $\dot{h}$. **Bottom:** Viscosity η as a function of the shear rate $\dot{\gamma}$.

membrane rigidity as the parasite goes through its asexual cycle. As for the higher parasitemia (4,5% and 9,5%), the errors in the viscosity plot in Fig. 7 shown that there is no significant difference between the samples.

Regarding the iRBCs, similar behaviour than in Fig. 7 is shown in the bottom plot of Fig. 8. In this case, the viscosity of the uninfected blood is clearly higher than in the first experiment (bottom plot of Fig. 7). However, this viscosity change is related to a time difference between each experiment of about two weeks, where the blood could have easily aged and increased its viscosity. With respect to the infected blood, the n exponent also approaches the Newtonian exponent of 1 as the parasitemia is increased, even reaching values of n over 1. This surpassing n value indicates that the fluid becomes shear-thickenning, so the viscosity increases as the shear rate applied increases. The quantitative separation between each curve is more pronounced in this second experiment, compared to the top plot of Fig. 7. Consequently, the difference in viscosity between each curve is larger, indicating that the blood, during this time of the week, was more susceptible to changes.

D. The effects of mature stages

In addition to the experiments to perform an early diagnostic of the disease, we performed experiments with blood infected with parasites at the late states of their asexual cycle. These mature forms consist basically on trophozoites and schizonts.

The results in Fig. 9 show similar results than in the last section. As the parasitemia of mature stage iRBCs is increased, the viscosity of blood decreases and becomes

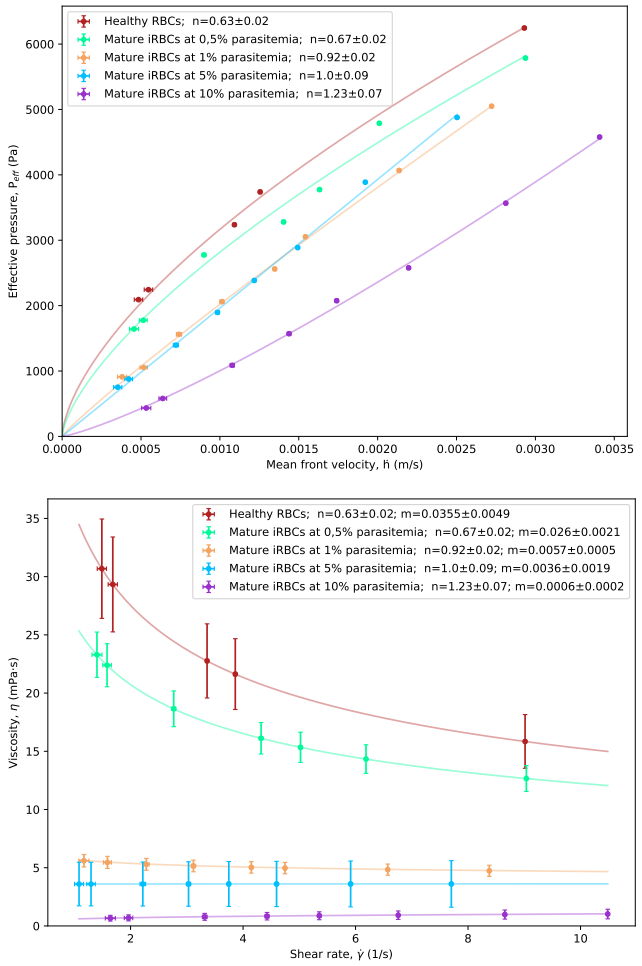

FIG. 9. Plots of the samples analysed to study the effect of mature forms in iRBCs, for different parasitemias. The obtained n and m parameters are shown in the legend, along side their error. **Top:** Effective pressure P_{eff} as a function of the mean front velocity $\dot{h}$. **Bottom:** Viscosity η as a function of the shear rate $\dot{\gamma}$.

more Newtonian. In the late stages of the cycle, the parasite becomes more stiff, so we expected an increased viscosity of the infected blood. The interaction between specific proteins of the parasite can lead to the binding of late-stage iRBCs to healthy RBCs, forming clusters known as rosettes [19]. This big clumps should increase the viscosity of blood, but the plots in Fig. 9 show the opposite.

E. Discussion

The plots obtained in Fig. 5 and in Fig. 6 show interesting results regarding the changes in viscosity when the RBCs are in the RPMI medium and when the sample is at human temperature. The results on the effect of temperature show that the viscosity decreases as the temperature increases, a behaviour that is supported by the results in [18].

With respect to the effect of the medium in blood rheology, no studies have been performed to corroborate the results obtained in this work. However, the viscosity difference between the samples of RBCs in RPMI and in plasma shown in Fig. 5 are reasonable from a rheological point of view. Firstly, numerous studies show that plasma viscosity is higher than water's [20], so the viscosity when adding RBCs should be higher for the plasma sample due to its viscosity. Secondly, plasma contains proteins like fibrinogen that increase the probability of *rouleaux* formation, these stacks of RBCs that ultimately increase the viscosity of blood. This aggregation effect has to be less noticeable in the RBCs in RPMI sample, since the formation of *rouleaux* is less favourable.

The results obtained for the *Pf* infected samples are surprising and non-expected. The studies on RBC deformability when infected by *Pf* show that the parasite increases the rigidity of the RBC and produce higher aggregation between them and with the environment [21]. Since the viscosity of blood strongly depends on the viscoelastic properties of the RBCs, our first hypothesis was that the viscosity of infected blood rises as the parasite matures and as parasitemia increases. This hypothesis was also based on the fact that the parasite causes rosetting (aggregation of healthy RBCs around an iRBC), which should increase the viscosity of blood since these aggregations are very stiff and prone to adhere to surrounding surfaces. Moreover, the iRBCs produce cytoadherence, that can cause microvascular obstructions in humans, hence hindering the blood flow and increasing its viscosity. Despite this, in our experiments using the microchannel, the cytoadherence should not be noticeable unless there are interactions between the RBCs and the walls of the microchannel or microtube.

Nevertheless, the results shown in Fig. 7, Fig. 8 and Fig. 9 are not consistent with the initial hypothesis. These plots show that the viscosity of infected blood decreases as the parasitemia is increased. Furthermore, the n exponent increases as the number of parasites in the sample increase; the shear-thinning behaviour disappears as the parasitemia rises. This results can be seen in both rings and mature stages iRBCs, and suggest that there is lysis in the samples analysed. It is well known that mature stages of the parasite induce the destruction of the RBC membrane,and that the RBCs at ring stages can also be destroyed by immune cells, so the decrease in viscosity could be explained by the induced lysis caused by the parasite.

These changes in viscosity could also be caused by the loss of RBCs when analysing the sample. In the beginning of the microchannel, since the microtube enters perpendicular to the microfluidic channel, the RBCs tend to slightly accumulate. This possible accumulation could be the reason why the RBCs do not flow properly and instead we are measuring the viscosity of plasma with less

RBCs. Regarding the rheometer, the microfluidic chip could also be the cause of this viscosity reduction, since due to the constant usage, the microchannel experiences degradation. All the measurements in this study have been done using two microchannels with the same geometry, that after many measurements the surfaces tend to get imperfections. Also, the constant cleaning and filling of the microchannel causes the bond between the bottom glass and the PDSM channel to weaken, worsening the measurements. However, this explanation is less likely to occur since the microrheometer has been used in multiple experiments, showing excellent results [6].

Another possible reason could be the ageing of the sample at 37°C. Since every set of measures took a long time (between 1 and 2 hours, if done properly), the samples that have previously been prepared could be altered due to their conservation at this temperature. These samples where static inside the incubator, which are ideal conditions for the parasite to cause lysis on the healthy RBCs and, for instance, reduce the hematocrit of the sample. This is an severe ageing effect that could be affecting the viscosity curves in these experiments.

Nonetheless, other biological reasons could explain the results obtained in Fig. 7, Fig. 8 and Fig. 9. Depending on the conditions, the increased rigidity could allow the iRBCs to flow more easily, resulting in a decreased viscosity. If the adherence conditions are not ideal for the iRBCs, the more rigid iRBCs could flow more easily through the plasma compared to the healthy RBCs, that are unaffected by the parasitation of *Pf*. Moreoever, as the parasite reaches its mature stages, the iRBCs become more spherical [10] and could lose the ability to aggregate in *rouleaux*, decreasing the overall viscosity. Another potential explanation is hemodilution, characterized by an expansion of plasma volume, may also contribute to decreased viscosity, as the diluted blood flows more freely.

V. CONCLUSIONS

In conclusion, this study aimed to investigate the effects of malaria infection on the viscosity of blood samples using a rheometer based on microfluidic principles. The results obtained revealed interesting findings and raised new questions for further research. The effects of the culture medium and the temperature on the viscosity blood were also studied.

The analysis of the culture RPMI medium showed that the medium used significantly affects the rheological properties of blood. Comparisons between RBCs in RPMI medium and RBCs in plasma demonstrated a considerable decrease in viscosity when using the RPMI medium. This highlights the importance of considering the medium composition when conducting rheological experiments on blood; yet, more experiments with infected blood need to be done to obtain conclusive results.

Temperature was found to have a notable impact on blood viscosity. The measurements performed at 37°C showed a decrease in viscosity compared to samples measured at lower temperatures. This observation aligns with existing knowledge on the relationship between temperature and blood viscosity.

This study also explored the potential of using viscosity measurements as an early diagnostic tool for malaria infection. By comparing viscosity curves of infected and non-infected blood samples, we aimed to identify characteristic differences that could indicate the presence of *Plasmodium falciparum* parasites during ring stages, circulating in natural conditions. The results revealed a decrease in viscosity with increasing parasitemia, contrary to the initial expectations. The viscosity curves showed a shift towards Newtonian behaviour and a decrease in the n exponent as parasitemia increased. These unexpected findings suggest the possibility of lysis occurring in the samples, potentially due to factors such as sample degradation, sample ageing at 37°C, or the accumulation of RBCs in the microchannel.

Furthermore, the effects of mature stages of malaria parasites on blood viscosity were investigated. Similar to the findings in the early diagnostic study, the viscosity of infected blood decreased as the parasitemia of mature stage parasites increased. This behaviour was contrary to the initial hypothesis, which expected increased viscosity due to factors such as increased membrane rigidity, rosette formation and cytoadherence. This reduction of viscosity could be caused by the lysis of RBCs, induce by the trophozoites and schizonts.

Overall, the unexpected findings regarding the effects of malaria infection at different stages highlight the complex nature of blood rheology and the need for further investigation. Future research should focus on elucidating the underlying mechanisms responsible for the observed viscosity changes in infected blood..

These findings contribute to the understanding of this parasite from a rheological point of view and may have implications for the development of rapid diagnostic tools for malaria and other related diseases. All these tools could allow us to improve the quality of life of the population in endemic regions, and being an step closer to the eradication of this potentially life-threatening disease worldwide.

ACKNOWLEDGMENTS

I would like to deeply thank my thesis advisors, Aurora and Hernando, for their constant guidance and for the incredible opportunity to work on this very interesting and relevant topic. Their broad knowledge in these topics have raised my passion and enthusiasm on this subjects, keeping me always digging for new findings and discussions.

Besides, I want to express my sincere gratitude to all

the members in Aurora's group for helping me whenever I needed, and all the members in Hernando's group for teaching me a more biological point of view of this work and chatting with me whenever I needed. Being part of these groups have been a privilege. I specially want to give my gratitude to Marc for his invaluable help in meticulously and skillfully preparation of the samples for this scientific paper, but also want to give thanks to Oscar for aiding me whenever I did not understand my results.

Last but not least, I want to express my gratefulness to all my relatives: colleagues, friends, etc. As well as specially thanking my family and my partner for the emotional support and for listening to me whenever I was thrilled explaining new exciting results.

Overall, my huge appreciation to everyone involved for helping me in everything I needed. This has been a very challenging experience, yet I feel fulfilled with the work done. Nothing would have been possible without the support of everyone involved.

---

[1] World Health Organization. "World malaria report 2020: 20 years of global progress and challenges", *World Health Organization* (2020).

[2] A. F. Cowman, J. Healer, D. Marapana, K. Marsh. "Malaria: Biology and Disease", *Cell*, volume 167, number 3, pp. 610-624 (2016).

[3] M. Koch, K. E. Wright, *et al.* "*Plasmodium falciparum* erythrocyte-binding antigen 175 triggers a biophysical change in the red blood cell that facilitates invasion", *Proceedings of the National Academy of Sciences*, volume 114, number 16, pp. 4225-4230 (2017).

[4] E. Dekel, D. Yaffe, I. Rosenhek-Goldian *et al.* "20S proteasomes secreted by the malaria parasite promote its growth", *Nat Commun*, volume 12, number 1172 (2021).

[5] K. Matthews, E. S. Lamoureux, M. E. Myrand-Lapierre, S. P. Duffy, H. Ma. "Technologies for measuring red blood cell deformability", *Lab Chip*, volume 22, number 7, pp. 1254-1274 (2022).

[6] C. A. Trejo. "Front Microrheology of Biological Fluids", *Universitat de Barcelona*, PhD Thesis (2016).

[7] G. D. Sloop, Q. De Mast, G. Pop, J. J. Weidman, J. A. St Cyr. "The Role of Blood Viscosity in Infectious Diseases", *Cureus*, volume 12, number 2 (2020).

[8] A. Q. Cowan, D. J. Cho, R. S. Rosenson. "Importance of Blood Rheology in the Pathophysiology of Atherothrombosis". *Cardiovascular drugs and therapy*, volume 26, number 4, pp. 339-348 (2012).

[9] C. Wagner, P. Steffen, S. Svetina. "Aggregation of red blood cells: From rouleaux to clot formation", *Comptes Rendus Physique*, volume 14, number 6, pp. 459-469 (2013).

[10] R. Suwanarusk, B. M. Cooke, A. M. Dondorp, K. Silamut, J. Sattabongkot, N. J. White, R. Udomsangpetch. "The Deformability of Red Blood Cells Parasitized by *Plasmodium falciparum* and *P. vivax*", *The Journal of Infectious Diseases*, volume 189, number 2, pp. 190-194 (2004).

[11] M. Depond, B. Henry, P. Buffet, P. A. Ndour. "Methods to Investigate the Deformability of RBC During Malaria", *Frontiers in Physiology*, volume 10 (2020).

[12] C. Trejo-Soto, E. Costa-Miracle, I. Rodriguez-Villarreal, J. Cid, M. Castro, T. Alarcon, A. Hernandez-Machado. "Front microrheology of the non-Newtonian behaviour of blood: scaling theory of erythrocyte aggregation by aging", *Soft Matter*, volume 13, number 16, pp. 3042-3047 (2017).

[13] W. Ostwald. "Ueber die rechnerische Darstellung des Strukturgebietes der Viskosität", *Kolloid-Zeitschrift*, volume 47, pp. 176–187 (1929).

[14] L. Méndez-Mora, M. Cabello-Fusarés, J. Ferré-Torres, C. Riera-Llobet, S. Lopez, C. Trejo-Soto, T. Alarcón, A. Hernandez-Machado. "Microrheometer for Biofluidic Analysis: Electronic Detection of the Fluid-Front Advancement", *Micromachines*, volume 12, number 6, 726 (2021).

[15] C. Trejo-Soto, E. Costa-Miracle, I. Rodriguez-Villarreal, J. Cid, T. Alarcón, A. Hernández-Machado. "Capillary Filling at the Microscale: Control of Fluid Front Using Geometry", *PLOS ONE*, volume 11, number 4, pp. 1-18 (2016).

[16] C. Lambros, J. P. Vanderberg. "Synchronization of Plasmodium falciparum Erythrocytic Stages in Culture", *The Journal of Parasitology*, volume 65, number 3, pp. 418-420 (1979).

[17] P. T. Boggs, J. E. Rogers. "Orthogonal distance regression" *Contemporary Mathematics*, volume 112, pp. 183-194 (1990).

[18] P. W. Rand, E. Lacombe, H. E. Hunt, W. H. Austin. "Viscosity of normal human blood under normothermic and hypothermic conditions", *Journal of Applied Physiology*, volume 19, number 1, pp. 117-122 (1964).

[19] J. Molina-Franky, M. E. Patarroyo, M. Kalkum, M. A. Patarroyo. "The Cellular and Molecular Interaction Between Erythrocytes and Plasmodium falciparum Merozoites", *Frontiers in Cellular and Infection Microbiology*, volume 12 (2022).

[20] M. Brust, C. Schaefer, R. Doerr, L. Pan, M. Garcia, P. E. Arratia, C. Wagner. "Rheology of Human Blood Plasma: Viscoelastic Versus Newtonian Behavior", *Physical Review Letters*, volume 110, number 7 (2013).

[21] G. D. Sloop, Q. De Mast, G. Pop, J. J. Weidman, J. A. St Cyr. "The Role of Blood Viscosity in Infectious Diseases", *Cureus*, volume 12, number 2 (2020).